AUTOMATED CLOUD REMOVAL ON HIGH-ALTITUDE UAV IMAGERY THROUGH DEEP LEARNING ON SYNTHETIC DATA

An Undergraduate Research Scholars Thesis

by

RYAN WELLS

Submitted to the Undergraduate Research Scholars program at
Texas A&M University
in partial fulfillment of the requirements for the designation as an

UNDERGRADUATE RESEARCH SCHOLAR

Approved by Research Advisor: Dr. Zhangyang Wang

May 2019

Major: Computer Science and Engineering

TABLE OF CONTENTS

ABSTRACT

Automated Cloud Removal on High-Altitude UAV Imagery through Deep Learning on Synthetic Data

Ryan Wells
Department of Computer Science and Engineering
Texas A&M University

Research Advisor: Dr. Zhangyang Wang
Department of Computer Science and Engineering
Texas A&M University

New theories and applications of deep learning have been discovered and implemented within the field of machine learning recently. The high degree of effectiveness of deep learning models span across many domains including image processing and enhancement. Specifically, the automated removal of clouds, smoke, and haze from images has become a prominent and pertinent field of research. In this paper, I propose an analysis and synthetic training data variant for the All-in-One Dehazing Network (AOD-Net) architecture that performs better on removing clouds and haze; most specifically on high altitude unmanned aerial vehicles (UAVs) images.

ACKNOWLEDGMENTS

I want to thank my advisor, Dr. Atlas Wang, for his support of my research and dedication to his students. My introduction to the fundamentals of machine learning through Dr. Wang gave me an auspicious start, and having the privilege of studying under him has been an honor. His door has always been open when I have questions. During times when I was stuck, Dr. Wang's expansive knowledge and insight of the field allowed him to suggest creative directions by which I could search for solutions. Ultimately, his dedication to the craft has inspired me to persevere, even when solutions are not yet on the horizon.

Additionally, I would like to thank Dr. Murphy and her team at the Center for Robot-Assisted Search and Rescue for generously providing image data from the Kilauea, Hawaii volcano eruption. This dataset allowed me to see the field of dehazing from a different perspective and it's practical applications.

I would also like to thank my friends within the Texas A&M Department of Computer Science for their endless assistance and for pushing me to be the best version of myself.

Lastly, I would like to thank my family for their resolute support. Without their help, achievements such as these would not have been possible.

LIST OF FIGURES

LIST OF TABLES

TABLE Page

1. INTRODUCTION

1.1 Dehazing and Cloud Removal

As the use of satellite and unmanned aerial vehicle (UAV) imaging increases in volume and diversity of physical geography, the inspection and analysis of such imagery has become increasingly cumbersome. While there are many tasks by which the original satellite or UAV image would be optimal such as meteorology or atmospheric physics, there has been an increasing demand for viewing and analyzing image data at the ground level. The use of these images encompasses a wide range of crucial applications including disaster response, geographical planning, environmental monitoring, and transportation optimization. However, these applications, are made more difficult through the unpredictable obscurities created by clouds, smoke, or haze. In addition to being cumbersome to visually process such images with the naked human eye, these obscurities also decrease the performance of automated image processing [4]. This problem of haze, cloud cover, and smoke overlaying an image has sparked the field of study known as dehazing. The act of dehazing can be simply stated as the following; given an image with obscurities such as clouds, smoke or haze, generate a new image with such obscurities removed, but containing the same quality of content within the image. A simple demonstration dehazing can be seen in Figure 1.1.

Figure 1.1: An example of an image with haze and followed by the result after dehazing

1.2 Applications

Among the many applications, one of the primary that this paper outlines is the usage of high altitude unmanned aerial vehicle (UAV) imaging for disaster response, relief, and recovery [5]. For example, during 2018, Mount Kilauea in Hawaii erupted causing destruction and the need for disaster response teams. One of these teams was the Center for Robot-Assisted Search and Rescue (CRASAR), led by Dr. Robin Murphy, a Professor at Texas A&M University. This group captured a large amount of high resolution images, constructing a dataset of real-world images seen in practice, which are highlighted in this paper. These images span large landscapes of buildings, houses, roads and forestry, all of which are seen in practice during search and rescue applications. One of these images can be seen in Figure 1.2. Generally, such images are post-processed by utilizing algorithms such as the RX Spectral Detection Algorithm, implemented in CRASAR's Computer Vision Emergency Response Toolkit [6]. These post-processing models can be better leveraged in search and rescue situations if the images are clearer and the underlying data can

be more easily seen. Improving the performance and accuracy of these post-processing models as well as visual quality of the captured images is crucial to improving the odds of finding survivors and surveying damage.

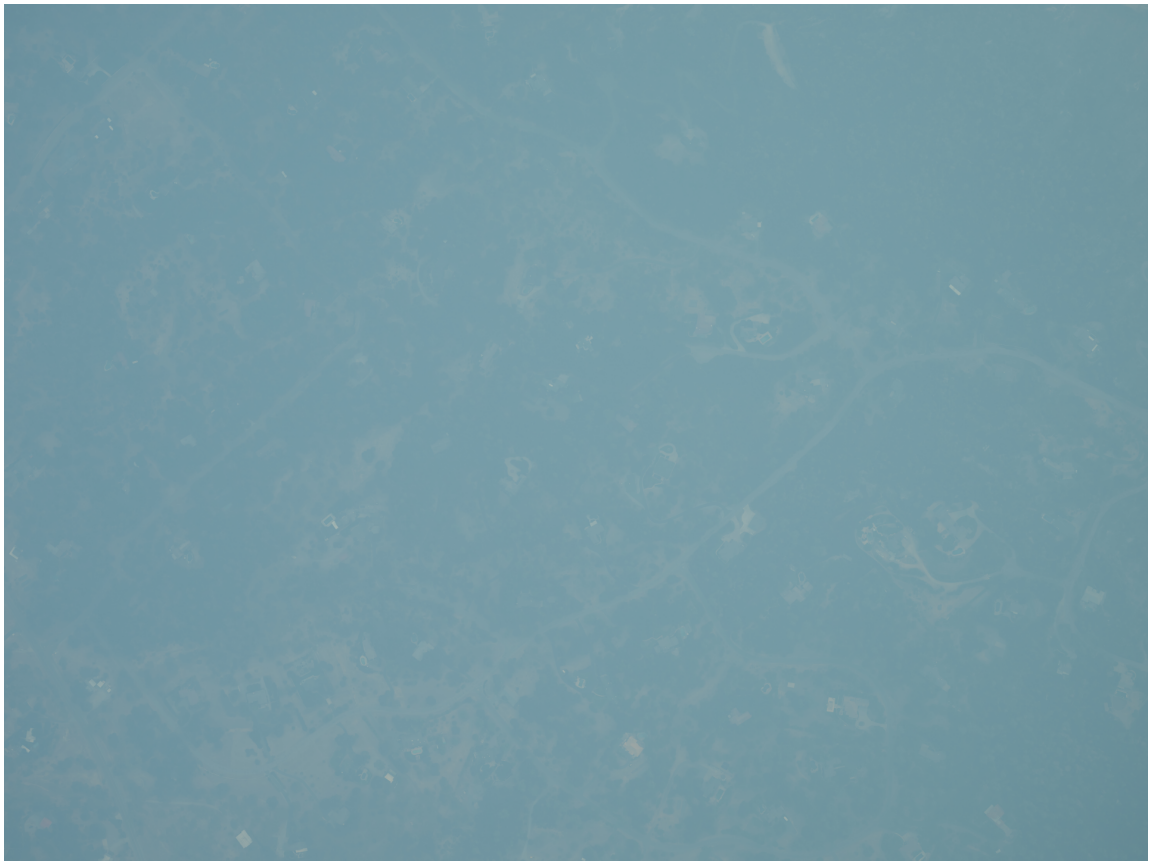

Figure 1.2: A real image sample from Dr. Murphy's team of a scene near the Mount Kilauea Eruption in May 2018.

Another application of dehazing on high altitude images is analysis of physical geography. For example researchers at the University of Tasmania utilized aerial photography captured by a UAV for monitoring landslides [7]. By capturing landscapes through several views, Lucieer et al. derived a 3D model of the mudslide that could be used to accurately

predict the particle dynamics during the landslide. Another group at University of Frankfurt captured high resolution UAV images for use on analysis of soil erosion in Morocco enabling better preparation on use of land [8].

These applications barely scratch the surface on the revolutionary use cases of UAVs and their ability to empower scientists and engineers to make better decisions. By improving the image quality captured in these environments through dehazing, these tasks can be improved in effectiveness.

1.3 Datasets

A critical component of supervised machine learning is the usage of paired datasets. In the case of dehazing hazy images, this means that both a hazy and dehazed image of the same scene must be captured. Unfortunately, acquiring a substantial number of photos from UAV's with both of these captured is impractical. Obtaining these images would entail taking photos of identical scenes during haze and haze-free conditions as well as eliminating the global light distortion component. Therefore, the optimal solution for supervised learning, given the available data, is to consider generating synthetic training data.

2. RELATED WORK

Throughout the past two decades, the field of dehazing has seen rapid progression in the techniques used for solving this problem. Each branch within this field has it's own unique method for solving this problem causing a variety of researchers with diverse specializations to contribute.

2.1 Image Enhancement and Fusion

Originally, methods for transforming the hazy images were based upon reversing the degradation of an image without regard to the causation of the haze. An example of one of the early pioneers of dehazing through image enhancement is *histogram equalization*. This algorithm aims to increase the dynamic range of gray within a grayscale image or the value within a color image within the HSV color space. For dehazing, this corrects images that are made too bright or dark by haze through correcting this distribution within a global or local patch, ultimately boosting the contrast [9]. Another example of an early image enhancement was known as *Retinex Theory*. This theory made the assumption that three sets of cone systems within the eye initially peak from three respective sets of light wavelengths. Additionally, the assumption is made that the human vision system discounts certain information about the entering light that would otherwise cause uncertainty about the illumination yet specifically pays close attention to the reflected object. This theory applies to dehazing through mimicking this process by estimating the ambient brightness and reversing it from the image [10].

Another high-performing method for dehazing is using image fusion. This method relies on generating multiple images with specific attributes corrected and then "fusing" or blending the corrected images together. A solution proposed by Ancuti et al. implements image fusion through combining two images I_1, I_2 with weight maps using Gaussian and

Laplacian Pyramids. I_1 is constructed through white-balancing, reducing the chromatic casts caused by atmospheric color. I_2 is constructed by pixel-wise subtraction of the mean global luminance, offsetting the darkness generally created on the underlying scene. This method differs from image enhancement algorithms like histogram equalization because domain knowledge such as atmospheric color bias and luminance of hazy images is included in this technique [11].

The computational efficiency of dehazing with histogram equalization, Retinex theory, and image fusion have have been proven to be computationally efficient. However, in terms of accuracy, recent advancements in models based upon deep learning have surpassed these approaches.

2.2 Deep Learning

Deep learning is a class of models loosely inspired by the human brain, by utilizing several stacked layers of non-linear processing units. Generally, these units are fed input from the previous layer, building a hierarchy of abstraction and ultimately resulting in approximating complex functions. This class of models has become increasingly popular in the past decade due to the availability of data and improvements in computing power. With the improvement in camera quality and availability of high resolution images, even more data can be utilized within an image.

Computer scientists, mathematicians, and atmospheric physicists have recently collectively implemented research combining the performance of deep learning models with insight on how the atmosphere and light therein, is distorted. Furthering this progress has been the usage of the *atmospheric scattering model*. As stated in "Vision and the Atmosphere", the atmospheric scattering model is a physical-based approach to modeling light by taking into account the global atmospheric light and the transmission matrix, the medium through which light travels [1].

Convolutional neural networks (CNNs) are a class of neural networks that utilize a convolution operator between layers rather than the matrix product of all weights in a fully connected neural network. This has allowed a reduction in the number of trained weights, especially in visual processing, and translation invariance. Among many interesting applications are the implementation of dehazing applied to dehazing using several architectures. For example, AOD-Net, a convolutional neural network designed by Li et al., is featured as the principal architecture implemented in this paper [12]. It is a convolutional neural networks that learns both the global light and transmission matrix under one function from the atmospheric scattering model and then inverts this function on a hazy image to generate a clean one. Another recent architecture proposed in CVPR 2018 was the Densely Connected Pyramid Dehazing Network (DCPDN) [13]. This network architecture is comprised of several dense blocks allowing for the network to extend deeper, yet also increases the number of weights needed to be learned [14]. Hence, the DCPDN requires more resources for training and is slower during test time. The DCPDN implements the same technique for inverting the haze from an image that was previously proposed in AOD-Net.

Another deep learning research area for dehazing is the recent flourishing field of *Generative Adversarial Networks* (GANs). GANs are generally comprised of two opposing neural networks, a discriminator and generator, with opposing goals. The goal of the generator network is to map a latent space to an ideal data distribution. The goal of the discriminator is to accurately determine whether it is being fed data that is real or constructed from the generator. This results in a zero-sum game between the generator and discriminator. Upon reaching a Nash equilibrium, the generator can effectively construct data mapping to the target domain.

GANs have made progress in the field of dehazing as well as cloud removal by applying the generator to construct hazy or cloudy images. The discriminator is then used

to classify the images as having been truly hazy or simply a construction of the generator. These models have been highly successful for improving images with nearly opaque blots caused by dense clouds due to their strong inpainting ability [15]. Enomoto et al., implemented a variant of a GAN known as the "Multispectral Conditional Generative Adversarial Network" (McGAN) which performs very well on dehazing images with dense and heterogeneous cloud obfuscation [16]. However, the primary drawback to this method, is that it requires an additional channel of information from the image: the near-infrared band (NIR). To capture data with the NIR band is more expensive, rare, and consumes additional battery for UAVs and satellites. By using NIR, the sense of structure of what is behind the clouds can be determined due to the greater cloud penetrability of NIR.

Because many of these models rely on learning the transmission matrix and atmospheric light through supervised learning, separate data outside the target images is required, known as training data in a supervised learning context. For standard convolutional networks, this paired training data is needed to compute the error during training. In the context of GANs, paired data is needed for initially training the baseline discriminator to establish a boundary for the target domain, before training the generator and discriminator together. Therefore, a reasonable amount of training data of the same scene with haze and without haze needs to be obtained to train such models. As stated in 1.3, this is a large reason for synthetically generating training data.

3. METHODS

3.1 Modeling Atmospheric Distortion

Over the past century, the atmospheric scattering model has been the standard in modeling how the atmosphere physically distorts the scene observed [1][17]. While it is based upon physics modeling light attenuation and scattering through the atmosphere, the same insight can be applied to the pixels within an image from an image-processing perspective. The model can be expressed succinctly as:

$$\mathbf{I}(x) = \mathbf{J}(x)t(x) + \mathbf{A}(1 - t(x)) \tag{3.1}$$

$$t(x) = e^{-\beta(\lambda)d(x)} \tag{3.2}$$

Where the captured image, $\mathbf{I}(x)$, can be defined as the sum of two components. The first component, $\mathbf{J}(x)$, is the scene radiance, which in dehazing, is defined as the haze-free image and is modified by $t(x)$, the transmission matrix. The product of these two elements, $\mathbf{J}(x)t(x)$, is commonly known as the *direct attenuation*. This models the effect by which the atmosphere degrades the information conveyed from the scene, due to light scattering and decay. The second component, $\mathbf{A}(1-t(x))$, is often is often referred to as the *airlight*. This models the effect of neighboring illumination produced by the environment resulting in intersecting light through the medium between the observer and scene, ultimately causing an additional shift in brightness. The transmission matrix, $t(x)$ is a function of the distance from the object to the camera, x, and the scattering coefficient, $\beta(\lambda)$. An empirical observation noted by Narasimhan et al. is that the dependency of β on wavelength (λ) is small enough to make the assumption that $\beta = \beta(\lambda)$ for most environments [1]. This model can be described within the RGB color space, visualized in Figure 3.1.

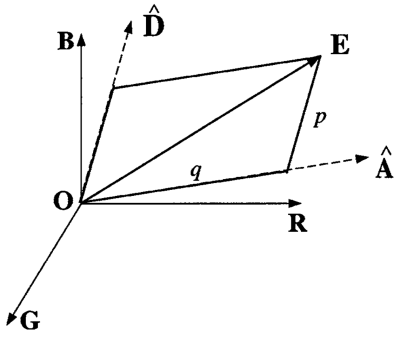

Figure 3.1: A visual representation of the atmospheric scattering model within the RGB color space from [1]. The color observed at a point, **E**, is a linear combination of the transmission color, $\hat{\mathbf{D}}$, and airlight color, $\hat{\mathbf{A}}$

3.2 Architecture

The primary network architecture employed for this task was the "All-in-One Dehazing Network" (AOD-Net), a lightweight convolutional neural network which approximates $\mathbf{J}(x)$ with respect to the atmospheric scattering model [12]. One of the large contributions of the AOD-Net was it's proposal of a function, $\mathbf{K}(x)$, that jointly expresses **A(1-t(x))** and **t(x)** which forces the network to converge on an optimal solution including both the direct attenuation and the airlight. The estimation of **K** occurs in the *K-Estimation* module in the AOD-Net. This module can be seen in Figure 3.2. The formulation for $\mathbf{K}(x)$ is constructed through first expressing Equation 3.1 in terms of the clean image:

$$\mathbf{J}(x) = \frac{1}{t(x)}\mathbf{I}(x) - \mathbf{A}\frac{1}{t(x)} + \mathbf{A}$$

As derived by Li et al., in [12], **J** can then be re-expressed in terms of **K** and a bias as:

$$\mathbf{J}(x) = \mathbf{K}(x)\mathbf{I}(x) - \mathbf{K}(x) + b \tag{3.3}$$

Where $\mathbf{K}(x)$ is a function of the hazy image, transmission matrix, and the global airlight:

$$\mathbf{K}(x) = \frac{\frac{1}{t(x)}(\mathbf{I}(x) - \mathbf{A}) + (\mathbf{A} - b)}{\mathbf{I}(x) - 1} \tag{3.4}$$

This function is then be approximated fully within the K-Estimation module through mean squared error (MSE) loss.

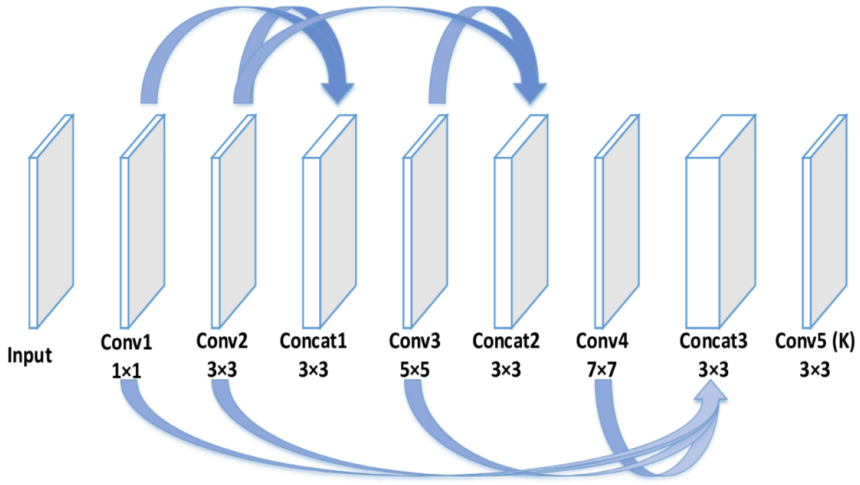

Figure 3.2: The *K-Estimation module* from the AOD-Net Paper [2]

3.3 Synthetic Data Generation

3.3.1 Atmospheric Lighting Variation

Atmospheric light variation through taking advantage of the atmospheric light scattering model, has been a popular technique in generation of synthetic haze. A vital component of the original All-in-One Dehazing paper was its' usage of atmospheric light variation for synthetic training data across haze-free images from the NYU2-Depth dataset [3]. The generated hazy and haze-free images comprised the paired training dataset for a controlled supervised training environment. Li et al. built the primary training set from

$1,449$ clean images, consisting of $27,256$ training hazy images, and $3,170$ testing images through varying the scattering coefficient, $\beta \in \{0.4, 0.6, 0.8, 1.0, 1.2, 1.4, 1.6\}$ [12]. One of these images is shown in Figure 3.3. A large drawback of this method is the requirement of utilizing the depth metadata within an image. Since the atmospheric scattering model heavily relies on the distance between the scene and the observer, a proper synthetic training dataset cannot be generated unless the distances are included or accurately predicted.

Figure 3.3: A comparison between haze generated by the atmospheric light scattering (Top) and Perlin noise (Bottom) on an image from the NYU2-Depth Dataset [3]

3.3.2 Perlin Noise

The proposed performance boost in UAV dehazing is completed by employing Perlin Noise to synthetically generate atmospheric haze. Perlin noise originated through a solution proposed to generate natural appearing textures during a time when textures seemed too "machine-like" [18]. By interpolating the dot product of random gradient vectors in a high-dimensional space, more natural textures can be created. An improvement to the original Perlin Noise algorithm was developed in 2001 called Simplex Noise which is nearly identical visually, yet lowers the computational cost from $O(2^n)$ to $O(n^2)$ for n dimensions. This is an important improvement because Perlin Noise that is visually utilized is commonly generated in higher dimensions. Two additional parameters, frequency and octave count, can be modulated to provide different types of textures. By increasing frequency, this increases the rate of samples taken, thus increasing the local volatility. The octave count refers to the accumulation of noise samples. By increasing the octave count, it increases the total variation of the noise, resulting in the noise looking more natural and fractal-like.

Two synthetic paired datasets were constructed using Perlin Noise[1] as the haze function. To generate the hazy image dataset, that better replicates clouds seen in UAV images, a combination of Simplex Noise and alpha-blending is applied in the following manner. Let $\mathbf{D}_i^{x,y}$ denote image i within a dataset of n haze-free images each of size x by y. Let $\mathbf{C}_{i,j}^{x,y}$ denote the hazy counterpart of $\mathbf{D}_i$ with j variants. Simplex Noise is generated in 3 dimensions with a frequency of 1024 and octave count of 512, resulting in a noise cube $\mathbf{N}^{x,y,z}$. A constant color bias, γ, is uniformly added to the simplex noise to prevent overly-darkening sections of the image. Empirically, the ideal bias was $\gamma = 200$ and the reasoning for adding this is discussed in section 5.2. A $2-$dimensional noise slice, $\mathbf{N}_z$, is then extracted

[1]Generation of the Perlin Noise was computed by the `noise` package `https://pypi.org/project/noise/`

at a random depth z from this cube. This is illustrated in Figure 3.4.

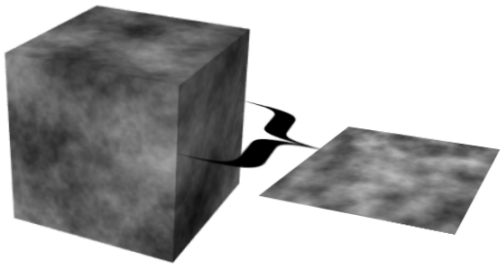

Figure 3.4: Generation of a noise cube followed by extracting a slice for 2-dimensional noise resembling a hazy atmosphere

To naturally synthesize the generated haze onto each $\mathbf{D}_i$, the noise slice, $\mathbf{N}_z$, is alpha-blended onto $\mathbf{D}_i$ to create $\mathbf{C}_{i,j}$ where:

$$\begin{cases} \mathbf{C}_{i,j} = \alpha \mathbf{N}_z + \beta \mathbf{D}_i \\ \alpha = 1 - \beta \\ \alpha \in .6, .7, .8 \end{cases}$$

In total, this resulted in $4,347$ generated training images from $1,449$ haze-free images in the NYU2-Depth dataset[2][3]. An example of a generated image can be seen in 3.3. An additional dataset was generated from the UC-Merced Land Use Dataset, constructing $6,300$ hazy images from $2,100$ haze-free images [19].

3.4 Training

Training was performed on AMD Ryzen 7 2700x @4.0GHz and a GeForce GTX 1080 Ti. The Atmospheric Light Variation training set (3.3.1) was trained for a total of 40 epochs

[2]During training time, a portion of these images were excluded for validation

with a batch size of 8, however it converged and performed well within approximately 10 epochs. The Perlin Noise (3.3.2) was trained for a total of 10 epochs with a batch size of 8, however it converged much more rapidly and could perform quite well even within a single epoch. This can be seen in Figure 3.5.

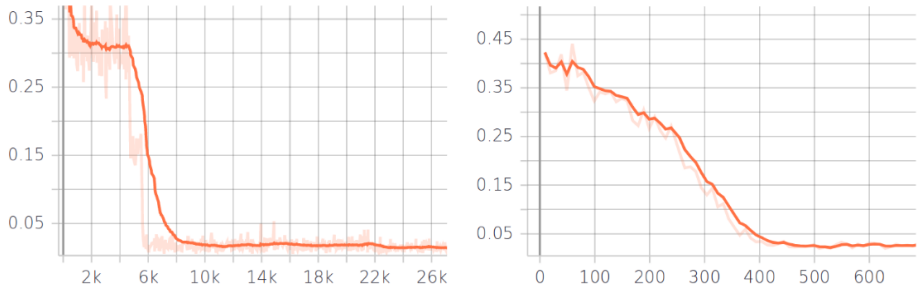

Figure 3.5: Training loss by iteration for Atmospheric Light Variation training set (3.3.1) on the left and Perlin Noise set (3.3.2) on the right

4. RESULTS

4.1 Subjective Visual Quality

The subjective visual quality is seen to improve when trained on the Perlin Noise based model. For example, in Figure 4.1 and Figure 4.2, the visual detail can be seen clearer due to higher contrast in the image.

Figure 4.1: From left to right, the original hazy image captured, the dehazed image using atmospheric scattering, the dehazed image using Perlin noise

Figure 4.2: A closer look at the images from Figure 4.1 demonstrating the original hazy image, atmospheric scattering, and Perlin noise data generation methods

4.2 Naturalness Image Quality Evaluator

The Naturalness Image Quality Evaluator (NIQE) is a powerful technique used in evaluating the distortion of a particular image based on statistical regularities present in normal images [20]. An image with an NIQE that is lower is considered to be closer to a naturally captured image, signifying it is less synthetic. Ideally, the act of dehazing should not destroy the natural aspect of the image. An NIQE analysis was performed[3] on a sample of dehazed images from CRASAR's Kilauea Dataset. As seen in Table 4.1, synthetic training on Perlin noise not only generates subjectively greater visually quality, but also performs greater quantitatively due to a lower NIQE.

Table 4.1: Mean NIQE Values of the Atmospheric Scattering and Perlin Noise Training Data Variants

Synthetic Training Data Variant	Mean NIQE
Atmospheric Scattering (3.3.1)	15.851
Perlin Noise (3.3.2)	**14.415**

4.3 Hough Transform Comparison

The Hough Transform is a method of extracting features within several domains including image analysis[21]. One of the popular applications of the Hough Transform is edge detection within an image. To compare the success of the synthetic training variants, Hough Transforms were run on the hazy and the dehazed images. The result can be seen in Figure 4.3. As a result, the Hough Transform could better detect the lines after having been trained on the Perlin Noise variant. This showcases improvements of attributes to

[3]The NIQE implementation used is: `https://github.com/aizvorski/video-quality`

an image that could particularly useful during live UAV image analysis or post-processing systems.

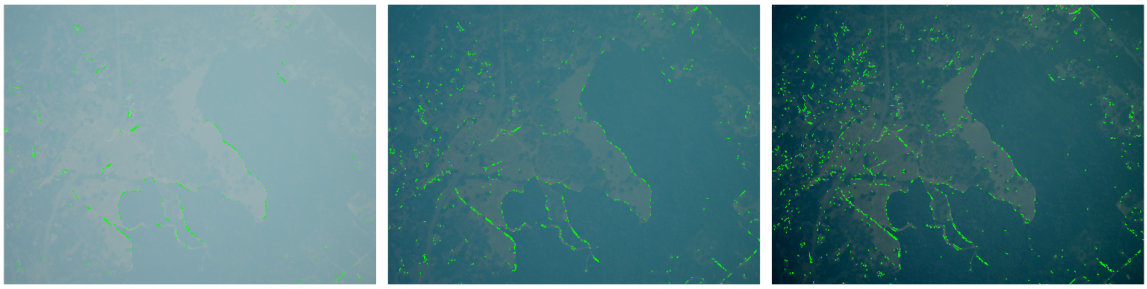

Figure 4.3: The resulting images after applying the Hough Transform. From Left to Right: Original Hazy Image, Atmospheric Scattering Training Variant, and Perlin Noise Training Variant

5. ANALYSIS

5.1 Why use the AOD-Net?

One of strong benefits of utilizing the AOD-Net is that it is lightweight in terms of layer count relative to many of the other CNN and GAN dehazing models. Also, the size of all of the model weights is less than 10 KB, meaning it relatively conservative in terms of memory usage. Like any other small model, it has the ability to run more efficiently on smaller devices like embedded systems or web browsers. The AOD-Net architecture is currently integrated on CRASAR's Computer Vision Emergency Response Toolkit[4].

With recent UAV and drone technology advancements, the possibilities of a dehazing model running on the UAV for real-time dehazing are only increasing. According to Li et al., the AOD-Net can significantly improve the accuracy of a Faster-R-CNN after dehazing an image[12]. Combining existing technologies such as object detection or object classification with a dehazing model on a UAV could potentially improve the accuracy when recognizing survivors or damage during search and rescue operations. Therefore, keeping the architecture lightweight was a major aspect of the decision for this task.

5.2 The relation between UAV Images and the Atmosphere

One of the properties of UAV images, is as the altitude increases, the variance of the point-wise distance between the observer and scene decreases. For most photograph dehazing, the variance between the scene and observer is quite high because photographers capture the subject and background which could have a large distance between them.

Another concept touched on in *Vision and the Atmosphere* is the behavior of airlight on the horizon [1]. With respect to the model 3.1, under high altitude conditions, the distortion

[4] `http://cver.hrail.crasar.org/`

of an image begins to have greater contribution from, **A**(1-t(x)), the airlight component. We can view how this occurs under extreme conditions such as determining the observed image **I** when the distance from scene to observer approaches ∞ under the atmospheric scattering model assumption:

$$\lim_{x\to\infty} \mathbf{I}(x) = \lim_{x\to\infty} \mathbf{J}(x)t(x) + \mathbf{A}(1 - t(x))$$

$$= \lim_{x\to\infty} \mathbf{J}(x)e^{-\beta(\lambda)d(x)} + \mathbf{A}(1 - e^{-\beta(\lambda)d(x)})$$

$$= \mathbf{A}$$

Clearly, the observed image is directly reduced to the airlight under extreme conditions, however it provides insight on the importance of **A** as the observer moves further from the scene. This is particularly important for UAV dehazing since the observer is distant for all points on the image. Because of this, it is most important to focus on providing an accurate measurement of **A**.

5.3 Why Perlin noise performs better

The Perlin noise synthetic training strategy has empirically demonstrated superior performance on hazy UAV images. I hypothesize that the primary cause was shifting the focus to establishing a minimum **A** across the training set through the introduction of a color bias, γ, during the noise generation. Within the atmospheric light scattering training variant, objects close to the observer can appear to have an almost near zero airlight term in many of the training samples. While this does increase training set diversity when operating in traditional photography, it adds unnecessary focus to the transmission matrix, which is a function of distance. Under the Perlin Noise variant, the transmission matrix is still estimated and benefits from the mutual refinement property outlined by Li et al., however, it is more forgiving due to the lesser dependence on x for UAV images. As derived in

Section 5.2, these types of images will likely observe an influence of $\mathbf{A}$ that only increases with altitude. The explanation for training data is that it not only attempts to capture the local stochastic nature of $t(x)$, but also the influence of $\mathbf{A}$ in UAV images.

6. CONCLUSION

In summary, the confluence of both increased UAV technology, combined with applications in Deep Learning, have resulted in significant research and advancement. The intersection of these two intriguing fields has produced the opportunity to solve the problem of dehazing UAV images. Throughout this research study, we saw many implementations and options to to address this problem. A brief survey of the utilization of high altitude image analysis show the impact that data assimilation from a new perspective can have. Additionally, a tour through the history of legacy image enhancement and recent techniques, illustrate the reasoning behind the continued push for improved quality of images.

With the recent exploration into the field of dehazing, as well as acquiring a real dataset from CRASAR's Kilauea, Hawaii drone analysis, we suggest a real world solution which aims to address the particular challenge of image quality. Through the application of a lightweight neural network, the AOD-Net, and the examination of new synthetic training methods, we found that a Perlin Noise-based approach was optimal.

Ultimately, the properties of haze within high altitude UAV images and increase in focus on the airlight term in the atmospheric model, reinforce the optimal nature of the approach.

REFERENCES

[1] S. G. Narasimhan and S. K. Nayar, "Vision and the atmosphere," *Int. J. Comput. Vision*, vol. 48, pp. 233–254, July 2002.

[2] B. Li, X. Peng, Z. Wang, J. Xu, and D. Feng, "An all-in-one network for dehazing and beyond," *CoRR*, vol. abs/1707.06543, 2017.

[3] P. K. Nathan Silberman, Derek Hoiem and R. Fergus, "Indoor segmentation and support inference from rgbd images," in *ECCV*, 2012.

[4] Y. Liu, G. Zhao, B. Gong, Y. Li, R. Raj, N. Goel, S. Kesav, S. Gottimukkala, Z. Wang, W. Ren, and D. Tao, "Improved Techniques for Learning to Dehaze and Beyond: A Collective Study," *ArXiv e-prints*, June 2018.

[5] M. F. Goodchild and J. A. Glennon, "Crowdsourcing geographic information for disaster response: a research frontier," *International Journal of Digital Earth*, vol. 3, no. 3, pp. 231–241, 2010.

[6] J. Proft, J. Suarez, and R. Murphy, "Spectral anomaly detection with machine learning for wilderness search and rescue," in *2015 IEEE MIT Undergraduate Research Technology Conference (URTC)*, pp. 1–3, IEEE, 2015.

[7] A. Lucieer, S. M. de Jong, and D. Turner, "Mapping landslide displacements using structure from motion (sfm) and image correlation of multi-temporal uav photography," *Progress in Physical Geography: Earth and Environment*, vol. 38, no. 1, pp. 97–116, 2014.

[8] S. d' Oleire-Oltmanns, I. Marzolff, K. Peter, and J. Ries, "Unmanned aerial vehicle (uav) for monitoring soil erosion in morocco," *Remote Sensing*, vol. 4, pp. 3390–3416, Nov 2012.

[9] W. Wang and X. Yuan, "Recent advances in image dehazing," *IEEE/CAA Journal of Automatica Sinica*, vol. 4, no. 3, pp. 410–436, 2017.

[10] E. H. Land and J. J. McCann, "Lightness and retinex theory," *Josa*, vol. 61, no. 1, pp. 1–11, 1971.

[11] C. O. Ancuti, C. Ancuti, and P. Bekaert, "Effective single image dehazing by fusion," in *2010 IEEE International Conference on Image Processing*, pp. 3541–3544, Sep. 2010.

[12] B. Li, X. Peng, Z. Wang, J. Xu, and D. Feng, "Aod-net: All-in-one dehazing network," in *The IEEE International Conference on Computer Vision (ICCV)*, Oct 2017.

[13] H. Zhang and V. M. Patel, "Densely connected pyramid dehazing network," in *Proceedings of the IEEE Conference on Computer Vision and Pattern Recognition*, pp. 3194–3203, 2018.

[14] G. Huang, Z. Liu, L. Van Der Maaten, and K. Q. Weinberger, "Densely connected convolutional networks," in *Proceedings of the IEEE conference on computer vision and pattern recognition*, pp. 4700–4708, 2017.

[15] R. A. Yeh, C. Chen, T. Yian Lim, A. G. Schwing, M. Hasegawa-Johnson, and M. N. Do, "Semantic image inpainting with deep generative models," in *The IEEE Conference on Computer Vision and Pattern Recognition (CVPR)*, July 2017.

[16] K. Enomoto, K. Sakurada, W. Wang, H. Fukui, M. Matsuoka, R. Nakamura, and N. Kawaguchi, “Filmy cloud removal on satellite imagery with multispectral conditional generative adversarial nets,” *CoRR*, vol. abs/1710.04835, 2017.

[17] M. Wang, J. Mai, Y. Liang, T. Z. J. Fu, Z. Zhang, and R. Cai, “Component-based distributed framework for coherent and real-time video dehazing,” *CoRR*, vol. abs/1609.02035, 2016.

[18] K. Perlin, “Improving noise,” in *ACM transactions on graphics (TOG)*, vol. 21, pp. 681–682, ACM, 2002.

[19] Y. Yang and S. Newsam, “Bag-of-visual-words and spatial extensions for land-use classification,” in *Proceedings of the 18th SIGSPATIAL International Conference on Advances in Geographic Information Systems*, GIS ’10, (New York, NY, USA), pp. 270–279, ACM, 2010.

[20] A. Mittal, R. Soundararajan, and A. C. Bovik, “Making a "completely blind" image quality analyzer,” *IEEE Signal Processing Letters*, vol. 20, pp. 209–212, March 2013.

[21] J. Illingworth and J. Kittler, “A survey of the hough transform,” *Computer vision, graphics, and image processing*, vol. 44, no. 1, pp. 87–116, 1988.